Solid-State NMR Spectroscopy of Paramagnetic Metallocenes[1]

Henrike Heise,[2] Frank H. Köhler,[3] and Xiulan Xie[4]

Anorganisch-chemisches Institut, Technische Universität München, D-85747 Garching, Germany
E-mail: f.h.koehler@lrz.tu-muenchen.de

   The paramagnetic metallocenes and decamethylmetallocenes $(C_5H_5)_2M$ and $(C_5Me_5)_2M$ with $M = $ V $(S = \frac{3}{2})$, Mn $(S = \frac{5}{2}$ or $\frac{1}{2})$, Co $(S = \frac{1}{2})$, and Ni $(S = 1)$ were studied by ^{1}H and ^{13}C solid-state MAS NMR spectroscopy. Near room temperature spinning sideband manifolds cover ranges of up to 1100 and 3500 ppm, and isotropic signal shifts appear between −260 and 300 ppm and between −600 and 1640 ppm for ^{1}H and ^{13}C NMR spectra, respectively. The isotropic paramagnetic signal shifts, which are related to the spin densities in the *s* orbital of ligand atoms, were discussed. A Herzfeld–Berger spinning sideband analysis of the ring carbon signals yielded the principal values of the paramagnetic shift tensors, and for metallocenes with a small *g*-factor anisotropy the electron spin density in the ligand π system was determined from the chemical shift anisotropy. The unusual features of the ^{1}H and ^{13}C solid-state NMR spectra of manganocene were related to its chain structure while temperature-dependent ^{1}H MAS NMR studies reflected antiferromagnetic interaction between the spin centers.   © 2001 Academic Press

   Key Words: solid-state NMR; paramagnetic metallocenes; spin density distribution; rotational sideband analysis.

INTRODUCTION

   In molecular paramagnetic compounds it often happens that the unpaired electrons are not concentrated at one center such as a transition metal. Rather they are partly transferred by direct delocalization and spin polarization to remote atoms where positive and negative spin density, respectively, can be detected. The spin density distribution within a molecule (*1*) is of particular interest for the understanding and the design of molecular magnetic materials (*2–6*), because intermolecular magnetic interactions depend on spin densities located at neighboring molecular sites (*7, 8*).

   Competing methods for the investigation of spin densities are (mostly polarized) neutron diffraction and magnetic resonance. Neutron diffraction is unique as it yields three-dimensional spin

maps of molecules (*9*). However, high experimental effort and thus costs do not allow the method to be applied routinely. The most common magnetic resonance method is EPR spectroscopy (*10*), which is well suited for the indirect detection of medium to large spin densities from experimental hyperfine coupling constants. Unfortunately, determination of the spin sign is not straightforward (cf. double- and triple-resonance methods (*11*)), and nonequivalent nuclei manifest themselves in multiplet splittings of the electron resonance, which are often not well resolved. For many compounds with suitable electron relaxation these weaknesses can be overcome by applying NMR spectroscopy (*12, 13*), because the sign of the signal shift is the same as that of the spin density at the nucleus and because the resolution may be better than 10^{-6}.

   The hyperfine interaction probed by magnetic resonance is a second-rank tensor, $\hat{A}$, with an isotropic contribution from the electron spin density located directly at the nuclear site, i.e., in the *s* orbital of the atom, and a traceless anisotropic contribution from unpaired electrons in *p* and *d* orbitals (*14*). In solution anisotropic parts of the hyperfine interaction are averaged out by random molecular reorientation, and valuable information about spin density in other orbitals is lost. In contrast, solid-state NMR spectroscopy also detects spin density in *p* and *d* orbitals that contribute to the total anisotropy of the signal shift. If the geometry of the molecule is known, a tensor analysis of the signals can give information about unpaired electrons outside the *s* core of the molecules (*15, 16*).

   In this context we were interested in applying solid-state NMR spectroscopy to open-shell bis(cyclopentadienyl)metal compounds (metallocenes), because they are promising building blocks for magnetic materials (*17, 18*) and because intermolecular magnetic interactions depend on the sign and the magnitude of the electron spin density in the π system of the cyclopentadienyl ligands (*8, 19–22*). It follows that determination of the π spin density is of considerable interest. A theoretical prediction can be made considering the frontier orbitals of these sandwich compounds (*23*) (Fig. 1). In metallocenes with more than 18 valence electrons (i.e., cobaltocenes and nickelocenes), the unpaired electrons occupy e_{1g}^* orbitals, which have considerable ligand contributions, and the spin density in the ligand π system must therefore be positive. In low-spin metallocenes with

---

198

Ⓐ
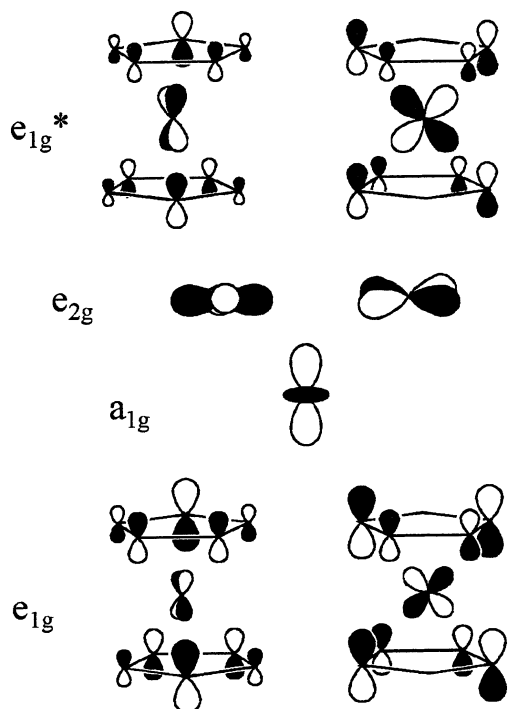
FIG. 1. Front orbitals of metallocenes. As the ligand centered part of the a_{1g} and e_{2g} orbitals is negligibly small, the Cp rings are not displayed in the figure.

less than 18 valence electrons (i.e., vanadocenes, chromocenes, and highly alkylated manganocenes) the unpaired electrons are located in the metal-centered e_{2g} and a_{1g} orbitals. In these compounds no virtually positive spin density is transferred to the ligand π system. Instead, polarization of the fully occupied bonding e_{1g} orbitals induces negative spin density in the π system. These features have been established experimentally for various substituted neutral and cationic metallocenes by solution NMR spectroscopy (19, 20). After some initial solid-state MAS NMR studies of chromocenes (24) and vanadocene (25) we now report on detailed studies of neutral paramagnetic first-row metallocenes and their permethylated analogues.

BACKGROUND

The interaction between an electron spin $\vec{S}$ and a nuclear spin $\vec{I}$ in an external magnetic field, $\mathbf{H}^{e,n}$, consists of two contributions: the hyperfine interaction with electron spin density located directly at the atom under study, $\mathbf{H}^{hf}$, and the dipolar interaction, $\mathbf{H}^{dip}$, with spin density well separated from the nucleus:

$$\mathbf{H}^{e,n} = \mathbf{H}^{hf} + \mathbf{H}^{dip}. \tag{1}$$

The hyperfine interaction is given by

$$\mathbf{H}^{hf} = \vec{I}\hat{A}\vec{S}. \tag{2}$$

The hyperfine interaction tensor $\hat{A}$ consists of an isotropic contribution, $\hat{A}_s$, (12, 13), which is proportional to the spin density in the s orbital of the atom,

$$\hat{A}_s = \frac{\mu_0}{3S} \cdot g_e\beta_e\gamma_n\rho_s \cdot \frac{1}{3} \cdot \hat{1}, \tag{3}$$

and an anisotropic contribution, $\hat{A}_p$ (14), which describes the dipolar interaction between a nuclear spin and the spin density in the atomic p orbital:

$$\hat{A}_p = \frac{\mu_0}{4\pi} \cdot g_e\beta_e\gamma_a\langle r_p^{-3}\rangle\rho_p\hat{a}. \tag{4}$$

Here μ_0 is the vacuum permeability, g_e is the electron g factor (considered isotropic, see below), β_e is the Bohr magneton, γ_n is the gyromagnetic ratio of the nucleus, ρ_s is the spin density in the s orbital (given in electrons per spatial unit), $\hat{1}$ is the unit matrix, $\langle r_p^{-3}\rangle$ is the expectation value of r^{-3} (r is the electron–nuclear distance) over the p orbital (for a $2p$ orbital of a carbon atom $\langle r_p^{-3}\rangle$ is 13.5 Å^{-3} (14)), ρ_p is the fraction of the electron spin S located in the p orbital of the atom under consideration, and $\hat{a}$ is an axially symmetric tensor with the main values $a_{||} = 4/5$ and $a_{\perp} = -2/5$ for the main axis of the orbital parallel and perpendicular to the external field, respectively. $\hat{A}_p$ is traceless as the orbital contribution at the nucleus is zero. The total hyperfine shift tensor (in ppm) is

$$\delta^{hf} = 10^6 \cdot \frac{g_e \cdot \beta_e \cdot S \cdot (S+1)}{\gamma_n \cdot 3k_BT} \cdot (\hat{A}_s + \hat{A}_p), \tag{5}$$

where k_B is the Boltzmann factor and T is the absolute temperature.

According to the point-dipole model, the dipolar interaction between the magnetic moments of an electron and a nuclear spin at a distance r is given by (15)

$$\mathbf{H}^{dip} = -\frac{1}{r^3} \cdot \langle\vec{\mu}_e\rangle\hat{D}\vec{\mu}_n = -\frac{1}{r^3} \cdot \gamma_n\langle\vec{\mu}_e\rangle\hat{D}\vec{I}, \tag{6}$$

where $\langle\vec{\mu}_e\rangle$ is the averaged magnetic moment of the electron spin,

$$\langle\vec{\mu}_e\rangle = \frac{\beta_e^2 S(S+1)}{3kT}\hat{g}\hat{g}\vec{B}_0,$$

$\vec{\mu}_n$ is the magnetic moment of the nuclear spin, $\hat{D}$ is an axially symmetric tensor with the main values $D_{||} = 2$ and $D_{\perp} = -1$, $\hat{g}$ is the electron g tensor, and $\vec{B}_0$ is the external magnetic field. The anisotropic dipolar shift (in ppm) is given by

$$\hat{\delta}^{dip} = 10^6 \cdot \frac{\mu_0}{4\pi} \cdot \frac{1}{r^3} \cdot \frac{\beta_e^2 S(S+1)}{3kT}\hat{g}\hat{g}\hat{D}. \tag{7}$$

If the g tensor is isotropic, the mean electron magnetic moment

is always parallel to the external magnetic field; the dipolar shift tensor is then traceless and axially symmetric. An anisotropic g tensor leads to an isotropic contribution to the dipolar shift, the so-called pseudocontact shift (26), and to a deviation from axial symmetry of $\hat{\delta}^{\mathrm{dip}}$. In addition, the $\hat{A}_s$ tensor defined in Eq. [3] becomes anisotropic (26, 27).

For paramagnetic metallocenes the total shift tensor obtained by solid-state NMR spectroscopy for a ring carbon atom is composed as

$$\hat{\delta}^{\mathrm{tot}} = \hat{\delta}^{\mathrm{dia}} + \hat{\delta}^{\mathrm{para}} = \hat{\delta}^{\mathrm{dia}} + \hat{\delta}^{\mathrm{hf}} + \sum_i \hat{\delta}_i^{\mathrm{dip}}. \qquad [8]$$

Here $\hat{\delta}^{\mathrm{dia}}$ is the chemical shift tensor of the isostructural diamagnetic ferrocene. Due to rapid reorientation of ferrocene and decamethylferrocene about the fivefold symmetry axis these chemical shift tensors are axially symmetric (28). The diamagnetic shift contribution for a given orientation defined by the angle χ between the external field and the molecular symmetry axis is given by

$$\delta^{\mathrm{dia}}(\chi) = \hat{\delta}_{\mathrm{iso}}^{\mathrm{dia}} + \frac{1}{3}\Delta\delta^{\mathrm{dia}} \cdot (3\cos^2\chi - 1), \qquad [9]$$

where $\Delta\delta^{\mathrm{dia}} = (\delta_{\|}^{\mathrm{dia}} - \delta_{\perp}^{\mathrm{dia}})$.

The effect of the unpaired electrons on the total shift anisotropy, $\hat{\delta}^{\mathrm{para}}$, consists of two contributions: the hyperfine interaction tensor $\hat{\delta}^{\mathrm{hf}}$ and the sum of all dipolar interactions with electron spin density at neighboring atoms i, $\sum_i \hat{\delta}_i^{\mathrm{dip}}$. For a ring carbon nucleus of a paramagnetic metallocene $\hat{\delta}^{\mathrm{hf}}$ is axially symmetric with respect to the main axis of the p_z orbital, which is parallel to the fivefold symmetry axis of the molecule (Fig. 2),

$$\delta^{\mathrm{hf}}(\chi) = \delta_{\mathrm{iso}}^{\mathrm{hf}} + \frac{1}{3}\Delta\delta^{\mathrm{hf}} \cdot (3\cos^2\chi - 1)$$

$$= \delta_{\mathrm{iso}}^{\mathrm{hf}} + \frac{2C}{5} \cdot \langle r_p^{-3} \rangle \cdot \rho_p \cdot (3\cos^2\chi - 1), \qquad [10]$$

where $\Delta\delta^{\mathrm{hf}} = (\delta_{\|}^{\mathrm{hf}} - \delta_{\perp}^{\mathrm{hf}})$ and C (in ppm · Å³) is

$$C = 10^{36} \cdot \left(\frac{\mu_0}{4\pi}\right) \cdot \frac{\beta_{\mathrm{e}}^2 \cdot S(S+1) \cdot \bar{g}^2}{3kT}. \qquad [11]$$

For the calculation of $\sum_i \hat{\delta}_i^{\mathrm{dip}}$ the fractions of electron spin at the centers of the metal $(1 - 10 \cdot \rho_p)$ and of the two adjacent ring carbon atoms (ρ_p at each neighbor) are considered as point dipoles. This is an approximation that neglects the spatial spin distribution around these centers; it is further discussed below. As the magnitude of dipolar coupling decreases with r^{-3}, dipolar interactions with spin density at more distant atoms or other molecules are neglected. The g factor is considered isotropic throughout this study. This assumption is justified for nickelocenes (29), vanadocenes (30), and cobaltocenes (31) with g
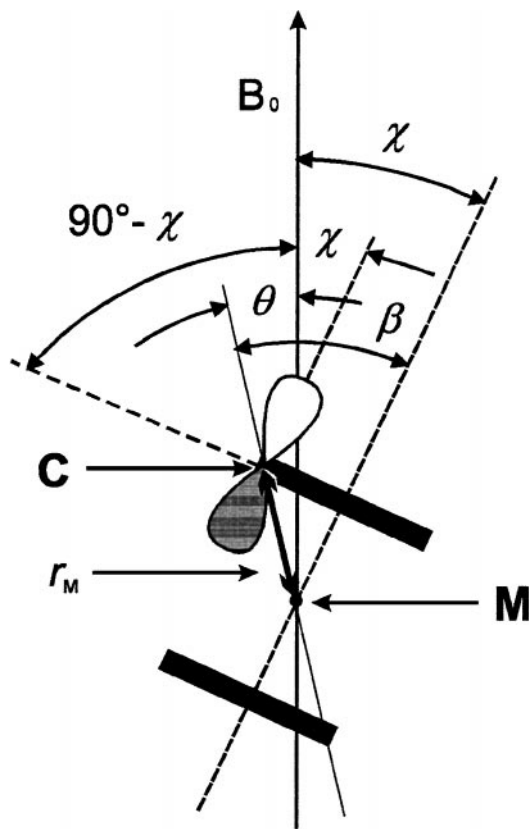
FIG. 2. Angles relevant for hyperfine and dipolar contributions to the chemical shift tensor of paramagnetic metallocenes. The sideview shows the cyclopentadienyl ligands as black bars, the metal M, and one selected ring carbon atom C. See text for details.

factor anisotropies <5%, so that in these cases the pseudocontact shift and the anisotropy of the contact shift (26, 27) can be neglected. It follows that the dipolar shift tensors $\hat{\delta}_i^{\mathrm{dip}}$ can be considered to be proportional to the dipolar tensor $\hat{D}$ (Eq. [7]). Furthermore, it follows that all $\hat{\delta}_i^{\mathrm{dip}}$ are axially symmetric with respect to the electron–nuclear distance vectors r_i, and the dipolar interaction, δ_M^{dip}, of a ring carbon nucleus with the electron spin at the metal atom M can be expressed by the tensor anisotropy $\Delta\delta^{\mathrm{dip}}$ and the angle θ between the electron–nuclear distance vector $\vec{r}$ and the external magnetic field:

$$\delta_M^{\mathrm{dip}}(\chi) = \frac{1}{3} \cdot \Delta\delta_M^{\mathrm{dip}} \cdot \langle 3\cos^2\theta - 1 \rangle$$

$$= r_M^{-3} \cdot C \cdot (1 - 10 \cdot \rho_p) \cdot \langle 3\cos^2\theta - 1 \rangle$$

$$= 0.5 \cdot r_M^{-3} \cdot C \cdot (1 - 10 \cdot \rho_p) \cdot (3\cos^2\beta - 1)$$

$$\cdot (3\cos^2\chi - 1). \qquad [12]$$

Due to rapid rotation about the fivefold symmetry axis the tensor is scaled by the factor $0.5 \cdot (3\cos^2\beta - 1)$ (32) where β is the angle between the vector r_M and the fivefold symmetry axis of the molecule (Fig. 2). Therefore, the resulting dipolar interaction

tensor has the same main axis as the chemical shift tensor and the hyperfine shift tensor. Analogously, the dipolar interaction with the electron spin density at each adjacent ring carbon atom, δ_C^{dip}, is given by

$$\delta_C^{dip}(\chi) = \frac{1}{3} \cdot \Delta\delta_C^{dip} \cdot \langle 3\cos^2(90° - \chi) - 1\rangle$$

$$= -0.5 \cdot r_C^{-3} \cdot C \cdot \rho_p \cdot (3\cos^2\chi - 1). \quad [13]$$

Note that r_C is perpendicular to the fivefold symmetry axis and hence its angle with the external magnetic field is $90° - \chi$, while $\langle 3\cos^2(90° - \chi) - 1\rangle$ becomes $0.5 \cdot \langle 3\cos^2 90° - 1\rangle \cdot \langle 3\cos^2\chi - 1\rangle$.

As all contributions to the shift tensor of a ring carbon atom are axially symmetric with respect to the fivefold symmetry axis, the shift tensor is fully characterized by its isotropic contribution δ,

$$\delta^{tot} = \delta^{dia} + \delta^{para}, \quad [14]$$

and its anisotropic contribution ($\Delta\delta = \delta_{||} - \delta_\perp$),

$$\Delta\delta^{tot} = \Delta\delta^{dia} + \Delta\delta^{para}.$$

With Eq. [8] applied to the metal and the adjacent two carbon atoms this yields

$$\Delta\delta^{tot} = \Delta\delta^{dia} + \Delta\delta^{hf} + \Delta\delta_M^{dip} + 2 \cdot \Delta\delta_C^{dip}. \quad [15]$$

According to Eq. [12] the term $\Delta\delta_M^{dip}$ is always positive, because ρ_p is smaller than 0.1. Furthermore, the sign of $\Delta\delta^{hf}$ and ρ_p is the same (see Eqs. [4] and [5]). As an important consequence, the ^{13}C chemical shift anisotropy of metallocenes depends on the sign of the spin density in the ligand π orbitals: If the sign is positive $\Delta\delta^{hf}$ adds to $\Delta\delta_M^{dip}$, and the width of the spinning sideband manifold is broad; if the sign is negative, $\Delta\delta^{hf}$ (partly) compensates $\Delta\delta_M^{dip}$, and the width is narrow. The magnitude of ρ_p can be calculated from $\Delta\delta^{tot}$ if the molecular parameters r_C, r_M, and β are known.

$$\rho_p = \left[\frac{\Delta\delta^{para}}{C} - 1.5 r_M^{-3}(3\cos^2\beta - 1)\right] \Big/ \left[1.2\langle r_p^{-3}\rangle \right.$$

$$\left. - 15 r_M^{-3}(3\cos^2\beta - 1) - 3 r_C^{-3}\right]. \quad [16]$$

Both the isotropic paramagnetic shift δ^{para} and the paramagnetic shift anisotropy $\Delta\delta^{para}$ depend on the sample temperature according to the Curie law. Therefore, a meaningful comparison of data requires conversion of these values to the reduced paramagnetic shift and shift anisotropy at the standard temperature of 298 K:

$$\vartheta_{298}^{para} = \delta_T^{para} \cdot T/298\,K \quad \text{and} \quad \vartheta_{298}^{para} = \Delta\delta_T^{para} \, T/298\,K. \quad [17]$$

EXPERIMENTAL

Samples were prepared by standard literature methods (*30*). All ^1H and ^{13}C NMR measurements were carried out with a Bruker MSL 300 spectrometer operating at 300.13 and 75.47 MHz, respectively, and with a 4-mm standard Bruker MAS probehead.

ZrO_2 and Si_3N_4 rotors were packed under inert gas with about 50 mg of sample and sealed with Kel-F caps. Although all compounds are strongly sensitive to oxygen and partly to moisture, no decomposition was observed during repeated measurements. The FIDs were sampled after applying single pulses (duration 4 μs). Delays of 8–10 μs for detector recovery were used, and repetition times were 200–400 ms. The signal-to-noise ratio was improved by exponential multiplication up to the matched filter, and baseline correction was applied. Signal shifts were measured relative to the external standard adamantane ($\delta(^1H) = 2.0$, $\delta(^{13}CH_2) = 29.5$). The temperature was determined by adding to each sample about 10 mg of nickelocene whose ^1H NMR signal shift was used as an internal thermometer. The procedure was analogous to that published for vanadocene (*25*); for nickelocene the data fit gave $T = -79477/(\delta^{exp} - 12.89\,ppm)$, the error was ± 1 K. Identification of the isotropic signal in spinning sideband manifolds was hampered, because the paramagnetic signal shifts depend on the sample temperature, which in turn depends on the spinning rate. Therefore, the sample temperature was kept constant at a value somewhat higher than that measured for the highest spinning rate, v_{rot}, while changing v_{rot}. As references for the isotropic diamagnetic shifts the solid-state MAS NMR spectra of ferrocene ($\delta(^1H) = 4.2$ ppm, $\delta(^{13}C) = 69.5$ ppm) and decamethylferrocene ($\delta(^1H) = 1.8$ ppm, $\delta(^{13}C_{ring}) = 78.8$ ppm, $(\delta(^{13}CH_3) = 10.4$ ppm) were recorded.

Sideband analyses according to Herzfeld and Berger (*33*) were carried out with the program Wsolids, HBA 1.2 (*34*). By using the tensor values so obtained the MAS NMR spectra were simulated with the program Wsolids 1 (*35*). The spin densities ρ_p given in Table 2 were calculated by using the following geometrical parameters and g factors: Cp_2V and Cp_2^*V: $r_M = 2.27$ Å, $r_C = 1.42$ Å, $\beta = 32.1°$ (*36*), $g = 1.9918$ (*30*); Cp_2Co: $r_M = 2.10$ Å, $r_C = 1.41$ Å, $\beta = 34.9°$ (*37*), $g = 1.764$ (*38*); Cp_2Ni and Cp_2^*Ni: $r_M = 2.16$ Å, $r_C = 1.38$ Å, $\beta = 32.9°$ (*39*), $g = 2.074$ (*29*).

RESULTS AND DISCUSSION

^1H and ^{13}C MAS NMR Spectra of Metallocenes

The ^1H and ^{13}C NMR spectra of nickelocene are shown in Figs. 3a and 3b, respectively. At a spinning rate of 16.1 kHz (associated with a sample temperature of 322.5 K) the ^1H and ^{13}C NMR signals are shifted to -234 and 1590 ppm, respectively, and the rotational sidebands cover a ranges of about 250 and 3000 ppm, respectively (see also Table 1). The spin density
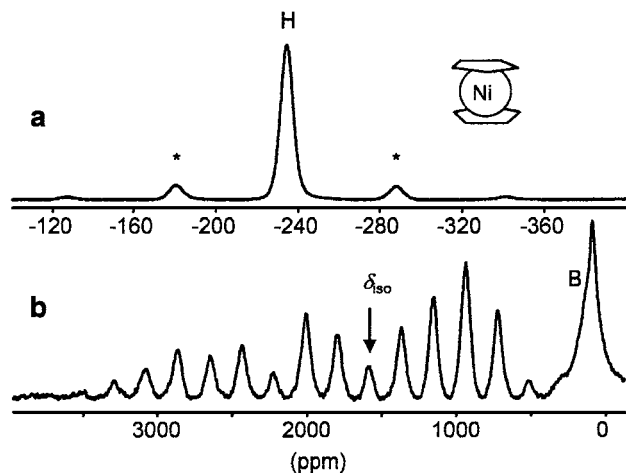
FIG. 3. ^{1}H (a) and ^{13}C (b) MAS NMR spectra of Cp$_2$Ni (322 K, spinning rate 16.1 kHz). In spectrum (a) spinning sidebands are marked with *. B is the background signal of the probehead.

at the ^{13}C nuclei and thus in the ligand π system is positive, while at the protons it is negative. The negative ^{1}H NMR signal shift is due to spin polarization, which induces negative spin density at the protons. Generally, positive paramagnetic shifts were found for the ^{13}C MAS NMR signals of ring carbon atoms when the metallocenes had 20 and 19 valence electrons, i.e., for (C$_5$Me$_5$)$_2$Ni, (C$_5$H$_5$)$_2$Co, and (C$_5$Me$_5$)$_2$Co (Table 1). ^{13}C NMR signals of the methyl groups of the decamethylmetallocenes (C$_5$Me$_5$)$_2$Ni and (C$_5$Me$_5$)$_2$Co and the ^{1}H NMR signal of (C$_5$H$_5$)$_2$Co have negative paramagnetic shifts while the proton NMR signal shifts of the methyl groups are positive. The signs of the spin density as derived from the signal shifts are in line

TABLE 1
Paramagnetic NMR Signal Shifts^a and Linewidths^b
of the Isotropic ^{1}H and ^{13}C NMR Signals of Metallocenes

|	C$_{ring}$	CH$_3$	H 1-5	CH$_3$
(C$_5$H$_5$)$_2$V	−491		302.5	
	(1.0)		(1.0)	
(C$_5$Me$_5$)$_2$V	−680	1340		118
	(6.0)	(15.0)		(5.2)
(C$_5$Me$_5$)$_2$Mn	17	−156		−1
	(1.1)	(1.0)		(3.3)
(C$_5$H$_5$)$_2$Co	618		−56.0	
	(1.2)		(1.0)	
(C$_5$Me$_5$)$_2$Co	556	−168		45
	(1.3)	(0.5)		(0.6)
(C$_5$H$_5$)$_2$Ni	1640		−257	
	(5.0)		(2.1)	
(C$_5$Me$_5$)$_2$Ni	1430	−594		224
	(2.5)	(0.7)		(1.8)
		−578		
		(0.7)		

^{a} In ppm at 298 K.
^{b} In kHz, in parentheses.

with the predictions mentioned in the Introduction and outlined in more detail in Refs. (*1, 19, 40*).

The ^{1}H and ^{13}C MAS NMR spectra of (C$_5$Me$_5$)$_2$V are displayed in Fig. 4. The ring carbon signal is shifted to −580 ppm with a sideband manifold spreading over 600 ppm. The ^{13}C NMR signal of the methyl group has a large high-frequency shift of 1340 ppm and is extremely broad with a half-width of 15 kHz. Finally, the ^{1}H NMR signal appears at 118 ppm. The signs of the paramagnetic signal shifts correspond to those expected for metallocenes with less than 18 valence electrons (*1, 19, 40*). Quite strikingly, the positive signal shift of the methyl carbon signal is roughly twice as large as the negative signal shift of the neighboring methyl ring carbon atom. This phenomenon is ascribed to delocalization into suitable σ orbitals of the Cp* ligand, which transfers positive spin to all nuclei (*20*). It adds to π polarization, which entails negative and positive spin at the ring and methyl carbon atoms, respectively. The net results are small and large signal shifts of the ring and methyl carbon atoms, respectively. Similarly, σ delocalization is responsible for the small positive signal shift of the ring carbon signal of decamethylmanganocene. Comparison of the ^{13}C MAS NMR spectra of nickelocene (Fig. 3b) and decamethylvanadocene (Fig. 4b) clearly shows the difference between the shift anisotropies of the ring carbon signals of metallocenes with more (nickelocene) and less (decamethylvanadocene) than 18 valence electrons. Despite the larger electron spin moment of vanadocene ($S = \frac{3}{2}$), the shift anisotropy of its ring carbon signal is only roughly one-third as large as that of the nickelocene ($S = 1$) ring carbon signal. This is in keeping with the interpretation of Eq. [16] (*vide supra*).

The ^{13}C NMR spectrum of (C$_5$Me$_5$)$_2$Ni (Fig. 5) shows two ^{13}C NMR signals for the methyl groups, while there is only one for the ring carbon atoms and for the protons, respectively. Most probably, this is due to two nonequivalent molecules in the asymmetric unit of the crystal, a feature that has been observed
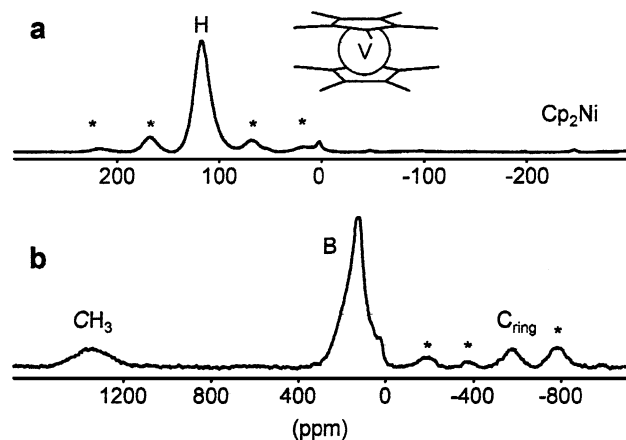
FIG. 4. ^{1}H (a) and ^{13}C (b) MAS NMR spectra of (C$_5$Me$_5$)$_2$V (307 K, spinning rate 15.0 kHz). Spinning sidebands are marked with *. Cp$_2$Ni is the internal temperature standard, and B is the background signal of the probehead.

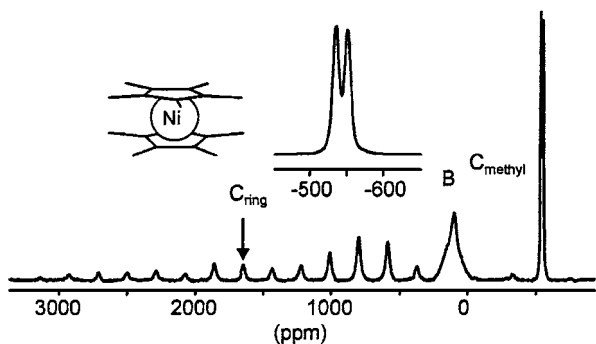**FIG. 5.** ^{13}C MAS NMR spectrum of (C$_5$Me$_5$)$_2$Ni (315 K, spinning rate 16.1 kHz). Nonassigned signals are spinning sidebands. The inset is an expansion of the methyl signal. B is the background signal of the probehead.

previously for decamethylchromocene (*24*). In the present case, the signal splittings expected for the ring carbon atoms as well as for the protons are not resolved at the given linewidths. For the decamethylmetallocenes (C$_5$Me$_5$)$_2$Co, (C$_5$Me$_5$)$_2$Mn, and (C$_5$Me$_5$)$_2$V only one set of signals was observed. This means that either these compounds crystallize differently or the signal splitting is not resolved.

In our previous publication on temperature-dependent NMR studies of solid vanadocene the reduced paramagnetic shift $\vartheta_{298}^{\mathrm{para}}$ of the ^{13}C NMR signal of Cp$_2$V was reported as -651 ppm (*25*). Now a thorough reinvestigation of the NMR spectra revealed that the largest spinning sideband was mistaken for the isotropic signal and that the true value is -491 ppm.

Tensor Analysis

The chemical shift tensor anisotropy for the ring carbon atoms of paramagnetic metallocenes is related to the spin density in the ligand π system (Eqs. [7] and [12]). If the g-factor anisotropy is negligibly small, the fraction of the total unpaired electron spin density located in one carbon p orbital of the ligand can be estimated with the help of Eq. [16]. Herzfeld–Berger spinning sideband analysis of the ^{13}C MAS NMR spectra of nickelocene obtained at spinning rates of 16.1 and 14.5 kHz (Figs. 6a and 6c) and at 322 K yielded a shift anisotropy of 2640 ppm and asymmetry parameters η of 0.19 and 0.20, respectively ($\eta = |\delta_{xx} - \delta_{yy}|/|\delta_{\mathrm{iso}} - \delta_{||}|$); further fitting results are collected in Table 2. The spinning sideband patterns of nickelocene simulated with the tensor values from Table 2 are displayed in Figs. 6b and 6d. There is good agreement between calculated and experimental patterns between about 600 and 2600 ppm, while at higher and lower frequencies the experimental intensities are too small. This may be explained by insufficient signal excitation far away from the irradiation center (at about 1600 ppm) even with pulse lengths as short as 4 μs. Slight errors may have been also introduced by nonideal baseline correction. The deviation of the shift tensors in Table 2 from axial symmetry may result from a small g-factor anisotropy, heteronuclear dipolar coupling, and distortions due to the anisotropy of the magnetic susceptibility (*41*). As for the effect of g-factor anisotropy, this would introduce errors via both the pseudocontact shift and the anisotropy of the contact shift (*26, 27*). The axial and equatorial g-factor components, $g_{||}$ and $g_\perp$, of solid nickelocene are 2.0023 and 2.11, respectively (*29*). This corresponds to a g-factor anisotropy of 5% and justifies the estimation of ρ_p from the shift tensor anisotropy. Another deviation may arise from the fact that the spin density is not localized strictly at the centers of the atoms as assumed by the point-dipole model mentioned under Background. Nonperfect localization would render the spin density estimated by Eq. [16] too small. More accurate results require full-space integration, an approach that is beyond the
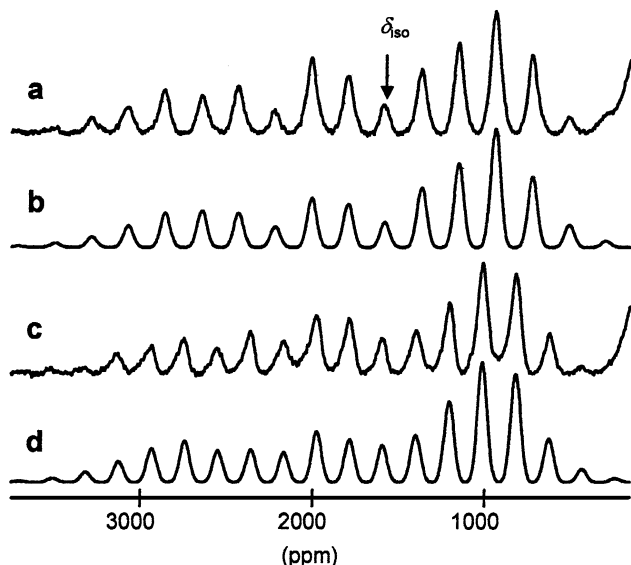

FIG. 6. ^{13}C MAS NMR spectra (a and c) and simulated spectra (b and d) of Cp$_2$Ni at 322 K and spinning rates of 16.1 kHz (a and b) and 14.5 kHz (c and d).

TABLE 2

Results of Herzfeld–Berger Analysis of the Ring Signals of Some Metallocenes from ^{13}C MAS NMR Spectra Obtained at Different Spinning Speeds

	T (K)	ν_{rot} (kHz)	δ^{iso} (ppm)	$\Delta\delta^a$ (ppm)	η^b	$\Delta\delta_T^{\mathrm{para}\,c}$ (ppm)	$\Delta\vartheta_{298}^{\mathrm{para}\,d}$ (ppm)	ρ_p^e (%)
(C$_5$H$_5$)$_2$V	306.0	14	-398	828	0.352	904	928	-0.43
	304.0	12	-408	795	0.000	871	889	-0.45
(C$_5$Me$_5$)$_2$V	307.0	15.0	-595	814	0.224	881	908	-0.44
(C$_5$H$_5$)$_2$Co	304.0	12	667	443	0.025	519	529	1.2
(C$_5$H$_5$)$_2$Ni	322.0	14.5	1594	2640	0.188	2716	2935	2.4
	322.3	16.1	1579	2641	0.201	2717	2939	2.4
(C$_5$Me$_5$)$_2$Ni	315.0	14.0	1436	2877	0.164	2944	3112	2.6
	315.0	16.0	1436	2943	0.095	3010	3182	2.7

^{a} $\Delta\delta = \delta_{zz} - (\delta_{xx} + \delta_{yy})/2$.

^{b} $\eta = (\delta_{yy} - \delta_{xx})/(\delta_{zz} - \delta_{\mathrm{iso}})$ with the tensor main values $|\delta_{zz} - \delta_{\mathrm{iso}}| \geq |\delta_{xx} - \delta_{\mathrm{iso}}| \geq |\delta_{yy} - \delta_{\mathrm{iso}}|$.

^{c} $\Delta\delta_T^{\mathrm{para}} = \Delta\delta - \Delta\delta^{\mathrm{dia}}$.

^{d} $\Delta\vartheta_{298}^{\mathrm{para}} = \Delta\delta_T^{\mathrm{para}} \cdot T/298$ K.

^{e} ρ_p: spin density in one carbon p orbital of the ligand (Eq. [16]).

scope of this paper. According to Eq. [16] the reduced paramagnetic shift anisotropy of nickelocene ($\Delta\vartheta_{298}^{\text{para}} = 2940 \pm 10$ ppm) corresponds to a population of $\rho_p = 2.4\%$ of the total electron spin in each carbon p orbital of the cyclopentadienyl ligands. In total, 24% of the unpaired electrons is transferred from the metal to the ligands. This is in reasonable accord with multiple-scattering X_α calculations (42), which gave an overall ligand contribution of 34% to the spin-containing orbitals of nickelocene.

For $(C_5H_5)_2V$, $(C_5Me_5)_2V$, $(C_5H_5)_2Co$, and $(C_5Me_5)_2Ni$, spinning sideband analyses of the ring carbon signal were also carried out (Table 2). It is gratifying that the maximal variation of the reduced paramagnetic shift anisotropies obtained from ^{13}C MAS NMR spectra at different spinning rates is 70 ppm for $(C_5Me_5)_2Ni$, which corresponds to only 3% of the total shift anisotropy; for Cp$_2$V the deviation is 30 ppm or 3.3%. The positive spin density in the ligand π orbitals of permethylated nickelocene amounts to 27%, which is somewhat more than for parent nickelocene. This corresponds to the increase of solution NMR signal shifts with an increasing number of methyl groups (19) and demonstrates that the solid-state NMR method provides rather detailed information as well. For cobaltocene $\rho_p = 1.2\%$ was found, which is again less than the theoretical value of 2.47% obtained by multiple-scattering X_α calculations (43). Within the error limits the same spin density of $\rho_p = -0.44\%$ of the total spin in each p orbital was found for both vanadocene and decamethylvanadocene. This agrees with theory, which predicts negative spin density in the ligand π system as a result of electron spin polarization (1, 19, 40).

Special Case: Solid Manganocene

Solid manganocene is unique among the metallocenes of the first transition metal period as it forms linear chains with terminal penta-hapto cyclopentadienyl ligands, and bridging cyclopentadienyl ligands that are di- and trihapto with respect to neighboring Mn atoms (see Fig. 7) (44). The metal-to-ligand bonds are weaker than in the case of other first-row transition metal metallocenes, and hence it is a high-spin compound ($S = \frac{5}{2}$). Magnetic measurements have revealed antiferromagnetic interaction between the spins (45).

The ^{1}H MAS NMR spectrum (Fig. 7a) of $(C_5H_5)_2$Mn, obtained at a spinning rate of 15 kHz, consists of one broad signal at 125 ppm (half-width $W = 2.1$ kHz) and a narrow one at -13 ppm ($W = 1.0$ kHz). The associated spinning sideband manifolds cover ranges of about 1100 and 600 ppm, respectively. Based on comparison with solution-state proton NMR spectra of mono- and dinuclear high-spin manganocene (46, 47) the signals at -13 and 125 ppm must be assigned to the protons of the terminal and bridging ligand, respectively. Since only one signal was found for the di- and trihapto moiety of the bridging ligand, it must be concluded that rapid haptotropic rearrangement occurs. While these findings confirm the chain structure of manganocene, more details follow from the fact that the pro-
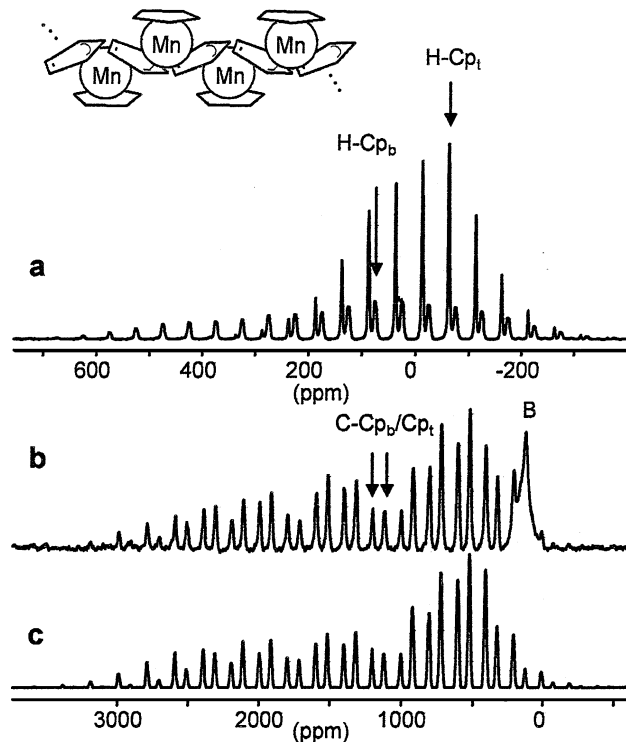
FIG. 7. (a) ^{1}H and (b) ^{13}C MAS NMR spectra of Cp$_2$Mn (308 K, spinning rate 15.0 kHz). Nonassigned signals are spinning sidebands. (c) Simulation of the ^{13}C MAS NMR spectrum. B is the background signal of the probehead.

ton shift anisotropy and linewidth of the terminal ligand are smaller than those of the bridging ligand. This points to shorter metal carbon distances of the bridging ligand, which leads to stronger electron–nuclear dipolar interactions and hence to enhanced shift anisotropy as well as to a faster nuclear relaxation (48, 49). Indeed, the average carbon–manganese distance of the bridging ligand is about 0.3 Å shorter than that of the terminal ligand (44). However, a reliable tensor analysis of the proton spectra is not possible, because strong homonuclear dipolar interactions render the line broadening homogeneous.

Temperature-dependent measurements of the ^{1}H MAS NMR spectrum showed some anomaly. According to Eq. [17] the reduced paramagnetic signal shift, $\vartheta_{298}^{\text{dip}}$, should be constant with temperature for simple paramagnetic molecules. By contrast, for manganocene $\vartheta_{298}^{\text{dip}}(^1H)$ increases as shown in Fig. 8. This is characteristic of antiferromagnetic interaction (50–53) and confirms magnetic measurements (45).

The ^{13}C MAS NMR spectrum of manganocene obtained at 15.0 kHz (Fig. 7b) also exhibits two signals at 1198 and 1116 ppm. Unlike the corresponding proton NMR signals they have the same signal half-width $W = 1.5$ kHz, and their shift difference is small, so that assignment to the bridging and terminal ligands is difficult. Both signals are associated with unusually large spinning sideband manifolds of about 3500 ppm. A tensor analysis of the spectra obtained at 13 and 15 kHz yielded
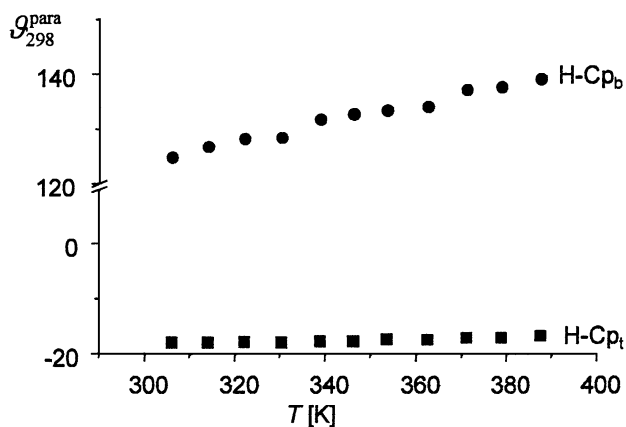
FIG. 8. Temperature dependence of the reduced paramagnetic proton signal shifts of solid manganocene.

shift anisotropies $\Delta\delta = 2315 \pm 40$ ppm for the low-frequency signal and $\Delta\delta = 2860 \pm 20$ ppm for the high-frequency signal with asymmetry parameters η below 0.3. The simulation of the experimental spectrum by using these data is shown in Fig. 7c. In order to estimate the electron spin density in the π system of the terminal ligand according to Eq. [16] the signal at 1116 ppm was assigned tentatively to that ligand. In addition, constant C (featuring in Eq. [16] and given in Eq. [11]) was adapted to antiferromagnetic interaction by introducing the effective magnetic moment μ_{eff},

$$C = 10^{36} \cdot \left(\frac{\mu_0}{4\pi}\right) \cdot \frac{\mu_{\text{eff}}(T)}{3kT}, \qquad [18]$$

where $\mu_{\text{eff}} = 4.673 \cdot \beta_e$ at 308 K (45), $r_{\text{MnC}} = 2.413$ Å, $r_{\text{CC}} = 1.378$ Å, and $\beta = 29.1°$ (44).

The spin density calculated in this way was $\rho_p = 0.18\%$ of the total electron spin $S = \frac{5}{2}$ in each carbon p orbital of the terminal ligand. Taking into account that direct spin delocalization is restricted to the e_{1g}^* orbitals and the two unpaired electrons therein, the contribution of the e_{1g}^* orbitals is $2.5 \cdot \rho_p = 0.45\%$ at each carbon p orbital. This value is significantly smaller than that found for nickelocenes and cobaltocenes, which is another indication of the comparatively weak covalent character of the metal–ligand bond in manganocene.

CONCLUSIONS

Solid-state MAS NMR spectroscopy proves to be a valuable method for the characterization of paramagnetic sandwich compounds. As for details of the *geometric* structure, the present study uncovers nonequivalent molecules in the unit cell, different bonding modes of the cyclopentadienyl ligand, and dynamic behavior. The *electronic* structure may be probed in detail by analyzing the isotropic signal shift and the spinning sidebands. The isotropic shift is related to unpaired electron density transferred to or induced in ligand orbitals with s-atomic orbital con-

tent and, therefore, gives information about spin delocalization mechanisms. From the spinning sidebands the spin density in the ligand π orbitals may be calculated. The analysis includes determination of the chemical shift anisotropy from the spinning sideband manifold, and its conversion to the anisotropic part of the hyperfine interaction tensor and subsequently to the spin densities. The results correspond to theoretical calculations, but limits of the method exist. Temperature-dependent studies show manganocene to experience antiferromagnetic interaction.

REFERENCES

1. F. H. Köhler, Probing spin densities by using NMR spectroscopy, *in* "Magnetism: Molecules to Materials" (J. S. Miller and M. Drillon, Eds.), pp. 379–430, Wiley-VCH, New York (2001).

2. O. Kahn, "Molecular Magnetism," VCH, New York, 1993.

3. E. Coronado, P. Delhaes, D. Gatteschi, and J. S. Miller (Eds.), "Molecular Magnetism: From Molecular Assemblies to the Devices," Kluwer Academic, Dordrecht (1996).

4. D. Gatteschi, Molecular magnetism: A basis for new materials, *Adv. Mater.* **6,** 635–645 (1994).

5. J. S. Miller and A. J. Epstein, Organic and organometallic molecular magnetic materials—Designer magnets, *Angew. Chem. Int. Ed. Engl.* **33,** 386–415 (1994).

6. S. Decurtins and R. Pellaux, Supramolecular host/guest compounds and their prospects for multifunctional materials, comments, *Inorg. Chem.* **20,** 143–161 (1998).

7. H. M. McConnel, Ferromagnetism in solid free radicals, *J. Chem. Phys.* **39,** 1910 (1963).

8. C. Kollmar and, O. Kahn, Ferromagnetic spin alignment in molecular systems: An orbital approach, *Acc. Chem. Res.* **26,** 259–265 (1993).

9. J. Schweitzer, *in* "Molecular Magnetism: From Molecular Assemblies to the Devices" (E. Coronado, P. Delhaes, D. Gatteschi, and J. S. Miller, Eds.), pp. 199–228, Kluwer Academic, Dordrecht, 1996.

10. J. A. Weil, J. R. Bolton, and J. E. Wertz, "Electron Paramagnetic Resonance," Wiley, New York, 1994.

11. H. Kurreck, B. Kirste, and W. Lubitz, "Electron Nuclear Double Resonance Spectroscopy of Radicals in Solution," VCH, New York (1988).

12. G. N. La Mar, W. DeW. Horrocks, Jr., and R. H. Holm, "NMR of Paramagnetic Molecules," Academic Press, New York (1973).

13. I. Bertini and C. Luchinat, NMR of paramagnetic substances in solution, *in* "Physical Methods for Chemists" (R. S. Drago, Ed.), pp. 500–556, Saunders College, Ft. Worth, TX (1992).

14. J. R. Morton and K. F. Preston, Atomic parameters for paramagnetic resonance data, *J. Magn. Reson.* **30,** 577–582 (1978).

15. A. Nayeem and J. P. Yesinowski, Calculation of magic-angle spinning nuclear magnetic resonance spectra of paramagnetic solids, *J. Chem. Phys.* **89,** 4600–4608 (1988).

16. A. C. Kolbert, R. Verel, H. De Groot, and M. Almeida, Determination of the spin density distribution in the organic conductor DMTM(TCNQ)$_2$ with ^{13}C magic angle spinning NMR, *Mol. Phys.* **91,** 725–730 (1997).

17. J. S. Miller, J. C. Calabrese, H. Rommelmann, S. R. Chittappeddi, J. H. Zhang, W. M. Reiff, and A. J. Epstein, Ferromagnetic behavior of TCNE.

Structural and magnetic characterization of decamethylferrocenium tetra-cyanoethenide, and decamethylferrocenium pentacyanopropenide, *J. Am. Chem. Soc.* **109,** 769–781 (1987).

18. J. S. Miller, A. J. Epstein, and W. M. Reiff, Ferromagnetic molecular charge-transfer complexes, *Chem. Rev.* **88,** 201–220 (1988).

19. J. Blümel, N. Hebendanz, P. Hudeczek, F. H. Köhler, and W. Strauß, Synthesis and NMR spectroscopy of metallocenium ions. Support for a new ferromagnetic coupling mechanism in decamethylmetallocenium tetracyanoethenides, *J. Am. Chem. Soc.* **114,** 4223–4230 (1992).

20. I. Gattinger, M. A. Herker, W. Hiller, and F. H. Köhler, Fusing rigid spin probes to paramagnetic sandwiches. Synthesis, crystal structures and NMR spectroscopy of bis(isocyclopentadienyl)metal compounds, *Inorg. Chem.* **38,** 2359–2368 (1999).

21. C. Kollmar and O. Kahn, Is the McConnel mechanism a suitable strategy for the design of molecular ferromagnets? *J. Am. Chem. Soc.* **113,** 7987–7994 (1991).

22. C. Kollmar, M. Couty, and O. Kahn, A mechanism for the ferromagnetic coupling in decamethylferrocenium tetracyanoethenide, *J. Am. Chem. Soc.* **113,** 7994–8005 (1991).

23. T. A. Albright, J. K. Burdett, and M.-H. Whangbo, "Orbital Interactions in Chemistry," Chap. 20.3, Wiley, New York (1985).

24. J. Blümel, M. Herker, W. Hiller, and F. H. Köhler, Study of paramagnetic chromocenes by solid-state NMR spectroscopy, *Organometallics* **15,** 3474–3476 (1996).

25. F. H. Köhler and X. Xie, Vanadocene as a temperature standard for ^{13}C and ^{1}H MAS NMR and for solution-state NMR spectroscopy, *Magn. Reson. Chem.* **35,** 487–492 (1997).

26. R. J. Kurland and B. R. McGarvey, Isotropic NMR shifts in transition metal complexes: The calculation of the Fermi contact and pseudocontact terms, *J. Magn. Reson.* **2,** 286–301 (1970).

27. I. Bertini, C. Luchinat, and G. Parigi, Hyperfine shifts in low-spin iron(III) hemes: A ligand field analysis, *Eur. J. Inorg. Chem.* 2473–2480 (2000).

28. D. Wemmer and A. Pines, Carbon-13 chemical shifts in solid metal sandwich compounds, *J. Am. Chem. Soc.* **103,** 34–36 (1981).

29. P. Baltzer, A. Furrer, J. Hulliger, and A. Stebler, Magnetic properties of nickelocene. A reinvestigation using inelastic neutron scattering and magnetic susceptibility measurements, *Inorg. Chem.* **7,** 1543–1548 (1988).

30. J. L. Robbins, N. Edelstein, B. Spencer, and J. C. Smart, Syntheses and electronic structures of decamethylmetallocenes, *J. Am. Chem. Soc.* **104,** 1882–1893 (1982).

31. L. Zoller, E. Moser, and J. H. Ammeter, EPR study of the electronic structure and dynamic Jahn–Teller-effect in decamethylmetallocenes, *J. Phys. Chem.* **90,** 6632–6638 (1986).

32. R. K. Harris, "NMR Spectroscopy — A Physicochemical View," Longman Scientific & Technical, Wiley, New York (1991).

33. J. Herzfeld and A. E. Berger, Sideband intensities in NMR spectra, *J. Chem. Phys.* **73,** 6021–6030 (1980).

34. HBA 1.2, K. Eichele and R. E. Wasylishen, Dalhousie University, Halifax, Canada.

35. WSolids1, K. Eichele and R. E. Wasylishen, Dalhousie University, Halifax, Canada.

36. M. Y. Antipin, K. A. Lyssenko, and R. Boese, Electron density distribution in the vanadocene crystal on the basis of X-ray-diffraction, *J. Organometal. Chem.* **508,** 259–262 (1996).

37. W. Bünder and E. Weiss, Verfeinerung der Kristallstruktur von Cobaltocen, *J. Organometal. Chem.* **92,** 65–68 (1975).

38. J. H. Ammeter, EPR of orbitally degenerated sandwich compounds, *J. Magn. Reson.* **30,** 299–325 (1978).

39. P. Seiler and J. D. Dunitz, The structure of nickelocene at room temperature, *Acta Crystallog. Sect. B* **36,** 2255–2260 (1980).

40. J. Blümel, P. Hofmann, and F. H. Köhler, NMR spectroscopy of paramagnetic complexes part 39. Natural abundance ^{2}H NMR of paramagnetic sandwich compounds, *Magn. Reson. Chem.* **31,** 2–6 (1993).

41. C. P. Grey, C. M. Dobson, and A. K. Cheetham, Susceptibility matching in MAS NMR. Determination of hyperfine tensors from paramagnetic stannates. *J. Magn. Reson.* **98,** 414–420 (1992).

42. A. Goursot, E. Penigault, and J. Weber, Application of the multiple scattering Xα MO method to the determination of the electronic structure of metallocene compounds II. Nickelocene and its cation, *New J. Chem.* **3,** 675–681 (1979).

43. J. Weber, A. Goursot, E. Penigault, J. H. Ammeter, and J. Bachmann, Electronic structure of metallocene compounds. 3. Comparison of the results of multiple-scattering Xα calculations with various electronic observables of cobaltocene, *J. Am. Chem. Soc.* **104,** 1491–1506 (1982).

44. W. Bünder and E. Weiss, Die Kristallstruktur von Manganocen, eine polymere Verbindung mit Cp-Brücken, *Z. Naturforsch. B* **33,** 1235–1237 (1978).

45. E. König, V. P. Desai, B. Kanellakopulos, and R. Klenze, Magnetic properties of the quasi one-dimensional Heisenberg linear chain antiferromagnet manganocene, *Chem. Phys.* **54,** 109–113 (1980).

46. N. Hebendanz, F. H. Köhler, G. Müller, and J. Riede, Electron spin adjustment in manganocenes. Preparative, paramagnetic NMR, and X-ray study on substituent and solvent effects, *J. Am. Chem. Soc.* **108,** 3281–3298 (1986).

47. F. H. Köhler and B. Schlesinger, Spin crossover, dimerization, and structural dynamics of manganocenes probed by deuterium NMR spectroscopy, *Inorg. Chem.* **31,** 2853–2859 (1992).

48. N. Bloembergen and L. O. Morgan, Proton relaxation times in paramagnetic solutions. Effects of electron spin relaxation, *J. Chem. Phys.* **34,** 842–850 (1961).

49. I. Bertini, C. Luchinat, and E. Borghi, A Fourier transform NMR investigation of [nBu$_4$Z][MPh$_3$I$_3$](Z = N, P, M = Co, Ni), *Inorg. Chem.* **20,** 306–308 (1981).

50. H. Atzkern, P. Bergerat, M. Fritz, J. Hiermeier, P. Hudeczek, O. Kahn, B. Kanellakopulos, F. H. Köhler, and M. Ruhs, Dinuclear paramagnetic metallocenes bridged by silyl groups. Synthesis and intramolecular interaction. *Chem. Ber.* **127,** 277–286 (1994).

51. H. Atzkern, P. Bergerat, H. Beruda, M. Fritz, J. Hiermeier, P. Hudeczek, O. Kahn, F. H. Köhler, M. Paul, and B. Weber, Intramolecular magnetic and electrostatic interactions in stepwise trinuclear paramagnetic metallocenes, *J. Am. Chem. Soc.* **117,** 997–1011 (1995).

52. H. Hilbig, P. Hudeczek, F. H. Köhler, X. Xie, P. Bergerat, and O. Kahn, Ferro- and antiferromagnetic exchange in decamethylbimetallocenes, *Inorg. Chem.* **37,** 4246–4257 (1998).

53. P. Hudeczek, F. H. Köhler, P. Bergerat, and O. Kahn, Cationic decamethylbimetallocenes of cobalt and nickel: Synthesis, redox behavior and magnetic interaction, *Chem. Eur. J.* **5,** 70–78 (1999).